

## Inverse Wave Scattering of Rough Surfaces with Emitters and Receivers in the Transition Zone

Slimane Arhab<sup>1, \*</sup> and Gabriel Soriano<sup>2</sup>

**Abstract**—We deal with the problem of determining the profile of a perfectly conducting rough surface from single-frequency and multistatic data. The two fundamental polarizations are investigated, in a two-dimension scattering configuration. Emitting and receiving antennas are positioned on a probing line some wavelengths above the profile. It is shown how the boundary integral equation method can be adapted to the case where the antenna footprint is much wider than the rough part of the profile. The Newton-Kantorovich iterative inversion process is then performed on these synthetic data. Its accuracy and robustness to additive noise are studied in the context of random rough surfaces with correlation length smaller than the wavelength and slope root mean square up to 0.9.

### 1. INTRODUCTION

The problem of determining the roughness of a surface from scattering data is encountered in many applications in both microwave and optical domains. The microwave remote sensing of natural surfaces such as sea, sand, soils or snow [1] is a major topic in geoscience. The scattered field from a rough soil can also hinder the detection, localization and characterization of some buried objects. Optical profilers provide through several chromatic or interferometric technologies non-contact surface metrology for design characterization and process control [2].

Methods were developed to deal with the difficulties associated to this class of inverse problem [3], namely non-linearity and ill-posedness [4]. Most common approaches consider approximate surface scattering theories [5] for describing the interaction between the electromagnetic field and the roughness. Those single scattering approximations are of theoretical and practical importance, since they can often be inverted analytically. In the early nineties were published inversion schemes based on the small perturbation method [6–8], the Kirchhoff approximation [9, 10] and the Rytov approximation [11]. More recently, a scattered field correlation procedure was developed in the framework of the small perturbation theory to characterize both the surface roughness and buried objects [12]. Each method has its own validity domain [13], but they are all restricted to configurations (roughness, angles) where multiple scattering is negligible.

For the scattering from a rough surface, the boundary integral equation method [14, 15] is the most fitted and commonly used numerical solution of the rigorous direct scattering problem, since it requires only the surface to be sampled. This method was efficiently implemented in inverse scattering schemes for two-dimensional [6, 16, 17] and three-dimensional [18] scattering. However, one requisite of the method is that the incident field is a tapered wave, usually a gaussian beam. This is a way to avoid the unphysical scattering from the edges of the sampled surface. In this paper, another approach is followed [19], where the rough surface is a local deformation of a plane. Stability and convergence of this finite section method when the roughness becomes non-local was studied in [20]. A classical configuration

---

*Received 30 October 2015, Accepted 15 December 2015, Scheduled 2 January 2016*

\* Corresponding author: Slimane Arhab (slimane.arhab@univ-avignon.fr).

<sup>1</sup> Université d'Avignon et des Pays de Vaucluse, UMR 1114 EMMAH, Avignon Cedex 84018, France. <sup>2</sup> Aix-Marseille Université, CNRS, Centrale Marseille, Institut Fresnel UMR 7249, Marseille 13013, France.

in microwaves is addressed where a set of antennas positioned on a horizontal line successively illuminate the rough surface that stands some wavelengths below. On one hand, the antennas are too distant from the surface for evanescent waves to rule the interaction, as in near-field. On the other hand, that distance is too short for far-field regime to be reached. The antennas are in the transition or intermediate zone. The forward model is presented in Section 2 for both fundamental polarization cases. The paper is restricted to two-dimensional scattering and perfectly conducting profiles.

The inverse problem is solved iteratively with the Newton-Kantorovich method [21, 22]. To constitute the data set, emitters also function as receivers. The profile cannot be estimated directly from that data set. The inverse problem is thus recasted as an optimization problem. The solution is built up iteratively by successively solving the forward problem and a local linear inverse problem. With the locally rough plane approach, the forward problem can be accurately modeled despite the fact that the emitters footprints on the profile are much wider than the sampled part of the profile. The local linear inverse problem relies on the calculus of the Fréchet derivative of the non-linear scattering operator. Based on the reciprocity theorem, this calculus was first proposed in far-field configuration [23]. It is here adapted to localized emitters and receivers. The inverse problem is detailed in Section 3.

This inversion scheme is tested on synthetic data. Realizations of Gaussian random rough profiles with varied correlation length are reconstructed, starting from the undeformed plane. Influence of polarization is underlined. Note that unusually rough surfaces are investigated in this paper, with the will to push the method to its limits. Section 4 is devoted to these numerical results. The paper is concluded in Section 5.

## 2. FORWARD PROBLEM

### 2.1. Configuration of the Study

In a Cartesian coordinates system  $(O, x, y, z)$  the rough surface  $\Gamma$  is invariant along the  $Oy$  axis (see Figure 1). Its profile is described by the equation  $z = \eta(x)$ . The function  $\eta$  is twice differentiable and non-zero only for  $|x| \leq \mathcal{T}/2$ . The unit vector  $\hat{\mathbf{n}}$  normal to the surface is directed toward the air. The field of study is the  $y$ -component of the electric field in the TE case ( $\mathbf{E} = \psi_{\text{te}}(x, z) \hat{\mathbf{y}}$ ), while it is the  $y$ -component of the magnetic field in the TM case ( $\mathbf{H} = \psi_{\text{tm}}(x, z) \hat{\mathbf{y}}$ ). We assume a time dependence  $e^{-i\omega t}$  at a fixed angular frequency  $\omega$ .

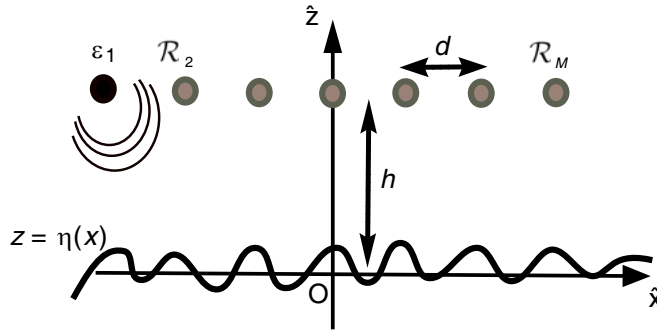


**Figure 1.** Geometry of the problem.

### 2.2. Incident Field

Let us now consider a set of  $\mathcal{M}$  antennas located along a horizontal line with an interdistance  $d$ , at a height  $h$  from the average plane  $z = 0$  of the surface. Each one of them plays the role of emitter and receiver but not simultaneously. When an antenna  $l$  acts like an emitter  $\mathcal{E}_l$ ,  $l \in \{1, 2, \dots, \mathcal{M}\}$  to illuminate the rough surface, all others act as receivers  $\mathcal{R}_m$ ,  $m \in \{1, 2, \dots, \mathcal{M}\}_{m \neq l}$  to measure the scattered field.

For the TE polarization, an emitter  $\mathcal{E}_\ell$  located at  $\mathbf{r}_\ell = x_\ell \hat{\mathbf{x}} + z_\ell \hat{\mathbf{z}}$  is set to produce an incident electric field on the point  $\mathbf{r} = x \hat{\mathbf{x}} + z \hat{\mathbf{z}}$  of space:

$$\mathbf{E}_{\text{inc}}^\ell = \psi_{i,\text{te}}^\ell(\mathbf{r}) \hat{\mathbf{y}} = -\frac{1}{4} \omega \mu_o H_0^{(1)}(k|\mathbf{r} - \mathbf{r}_\ell|) \hat{\mathbf{y}} \quad (1)$$

in order to mimic an electric dipole with moment oriented along the invariance direction  $\hat{\mathbf{y}}$  of the surface.  $H_0^{(1)}$  is the first-kind Hankel function of zero-order while  $k$  denotes the wavenumber in the air at angular frequency  $\omega$ .

Rotating the electric dipole of the emitter  $\mathcal{E}_\ell$  of a quarter turn in the  $(xOy)$  plane gives an electric dipole moment along  $\hat{\mathbf{x}}$ , that is associated to an illumination under the TM polarization:

$$\mathbf{H}_{\text{inc}}^\ell = \psi_{i,\text{tm}}^\ell(\mathbf{r}) \hat{\mathbf{y}} = -\frac{ik}{4} H_1^{(1)}(k|\mathbf{r} - \mathbf{r}_\ell|) \frac{z - z_\ell}{|\mathbf{r} - \mathbf{r}_\ell|} \hat{\mathbf{y}} \quad (2)$$

with  $H_1^{(1)}$  the first-kind Hankel function of first-order.

### 2.3. Boundary Integral Formalism

Since the surface is a local deformation of the horizontal plane, the total field  $\psi^\ell$  writes as the sum of the incident field  $\psi_i^\ell$  as defined previously and the field  $\psi_r^\ell$  that would be reflected by the horizontal plane according to the boundary conditions and the scattered field  $\psi_s^\ell$  that represents the contribution of the roughness.

$$\psi^\ell = \psi_i^\ell + \psi_r^\ell + \psi_s^\ell \quad (3)$$

This scattered field  $\psi_s^\ell$ , that satisfies a radiation condition in the air, has a Kirchhoff-Helmholtz integral representation in this half-space: for an observation point  $\mathbf{r} = x\hat{\mathbf{x}} + z\hat{\mathbf{z}}$  outside  $\Gamma$ ,

$$\int_{\Gamma} \left\{ \partial_n g(\mathbf{r}, \mathbf{r}') \psi_s^\ell(\mathbf{r}') - g(\mathbf{r}, \mathbf{r}') \partial_n \psi_s^\ell(\mathbf{r}') \right\} d\Gamma = \begin{cases} \psi_s^\ell(\mathbf{r}) & z > \eta(x) \\ 0 & z < \eta(x) \end{cases} \quad (4)$$

with  $\mathbf{r}' = x'\hat{\mathbf{x}} + \eta(x')\hat{\mathbf{z}}$  the integration point over  $\Gamma$ , or source point. The scattered field  $\psi_s^\ell(\mathbf{r})$  and its normal derivative  $\partial_n \psi_s^\ell(\mathbf{r})$  are taken at the limit from the air onto the surface. The free space Green's function in the air is  $g(\mathbf{r}, \mathbf{r}') = \frac{1}{4} H_0^{(1)}(k|\mathbf{r} - \mathbf{r}'|)$ , and  $\partial_n g(\mathbf{r}, \mathbf{r}') = \hat{\mathbf{n}}(\mathbf{r}') \cdot \nabla_{\mathbf{r}'} g(\mathbf{r}, \mathbf{r}')$  denotes its normal derivative with respect to the source point.

At the limit when the observation point  $\mathbf{r}'$  tends toward the profile, from air or from the metal, formula (4) leads to the integral equation:

$$\frac{1}{2} \psi_s^\ell(\mathbf{r}) - \int_{\Gamma} \partial_n g(\mathbf{r}, \mathbf{r}') \psi_s^\ell(\mathbf{r}') d\Gamma + \int_{\Gamma} g(\mathbf{r}, \mathbf{r}') \partial_n \psi_s^\ell(\mathbf{r}') d\Gamma = 0 \quad (5)$$

where both  $\mathbf{r}$  and  $\mathbf{r}'$  are points on the profile  $\Gamma$ . With two independent unknown surface densities  $\psi_s^\ell$  and  $\partial_n \psi_s^\ell$ , Equation (5) can only be solved with a supplementary equation, that is the boundary condition on the profile. Depending on the polarization case,

$$\psi_{\text{te}}^\ell = 0 = \psi_{i,\text{te}}^\ell + \psi_{r,\text{te}}^\ell + \psi_{s,\text{te}}^\ell \quad (6)$$

$$\partial_n \psi_{\text{tm}}^\ell = 0 = \partial_n \psi_{i,\text{tm}}^\ell + \partial_n \psi_{r,\text{tm}}^\ell + \partial_n \psi_{s,\text{tm}}^\ell \quad (7)$$

on any point of the profile  $\Gamma$ .

Therefore, the forward problem can be solved by means of two coupled equations. The first one, denoted as observation equation, relates the scattered field measured on the receivers to the unknown surface density. This unknown is obtained by solving the second equation, the so-called state equation, for a given profile-function and a well known incident field. We now summarize the two different polarization cases. Under the TE polarization, where the surface unknown is given by the normal derivative of the scattered field on the rough surface  $\partial_n \psi_{\text{te}}^\ell$ , the observation Equation (8) and the state Equation (9) write:

$$\psi_{\text{te}}^{m\ell} = \psi_{i,\text{te}}^{m\ell} + \psi_{r,\text{te}}^{m\ell} - \int_{\Gamma} g(\mathbf{r}_m, \mathbf{r}) \partial_n \psi_{s,\text{te}}^\ell(\mathbf{r}) d\Gamma - \int_{\Gamma} \partial_n g(\mathbf{r}_m, \mathbf{r}) (\psi_{i,\text{te}}^\ell(\mathbf{r}) + \psi_{r,\text{te}}^\ell(\mathbf{r})) d\Gamma \quad (8)$$

$$\int_{\Gamma} g(\mathbf{r}, \mathbf{r}') \partial_n \psi_{s,\text{te}}^\ell(\mathbf{r}') d\Gamma = \frac{1}{2} (\psi_{i,\text{te}}^\ell(\mathbf{r}) + \psi_{r,\text{te}}^\ell(\mathbf{r})) - \int_{\Gamma} \partial_n g(\mathbf{r}, \mathbf{r}') (\psi_{i,\text{te}}^\ell(\mathbf{r}') + \psi_{r,\text{te}}^\ell(\mathbf{r}')) d\Gamma \quad (9)$$

In TE polarization, receivers are sensitive to the total field  $\psi_{\mathbf{te}}^{m\ell} = \psi_{\mathbf{te}}^\ell(\mathbf{r}_m)$ , while it is the derivative with respect to the  $z$  variable  $\partial_z \psi_{\mathbf{tm}}^{m\ell} = \partial_z \psi_{\mathbf{tm}}^\ell(\mathbf{r}_m)$  in TM polarization, since measurement is proportional to the total electric field component along the receiver electric dipole moment. Therefore, the forward model in the TM case is

$$\partial_z \psi_{\mathbf{tm}}^{m\ell} = \partial_z \psi_{\mathbf{i},\mathbf{tm}}^{m\ell} + \partial_z \psi_{\mathbf{r},\mathbf{tm}}^{m\ell} + \int_{\Gamma} \partial_z g(\mathbf{r}_m, \mathbf{r}) (\partial_n \psi_{\mathbf{i},\mathbf{tm}}^\ell(\mathbf{r}) + \partial_n \psi_{\mathbf{r},\mathbf{tm}}^\ell(\mathbf{r})) d\Gamma + \int_{\Gamma} \partial_z \partial_n g(\mathbf{r}_m, \mathbf{r}) \psi_{\mathbf{s},\mathbf{tm}}^\ell(\mathbf{r}) d\Gamma \quad (10)$$

$$\frac{1}{2} \psi_{\mathbf{s},\mathbf{tm}}^\ell(\mathbf{r}) - \int_{\Gamma} \partial_n g(\mathbf{r}, \mathbf{r}') \psi_{\mathbf{s},\mathbf{tm}}^\ell(\mathbf{r}') d\Gamma = \int_{\Gamma} g(\mathbf{r}, \mathbf{r}') (\partial_n \psi_{\mathbf{i},\mathbf{tm}}^\ell(\mathbf{r}') + \partial_n \psi_{\mathbf{r},\mathbf{tm}}^\ell(\mathbf{r}')) d\Gamma \quad (11)$$

For both polarizations, the data set  $\mathcal{U}$  ( $\mathcal{U} = \{\psi_{\mathbf{te}}^{m\ell}\}_{m,\ell}$  or  $\mathcal{U} = \{\partial_z \psi_{\mathbf{tm}}^{m\ell}\}_{m,\ell}$ ) is related to the profile-function  $\eta$  via a non-linear operator  $\mathbf{F}$  involving the coupled equations of fields reported in (8) and (9) for TE polarization and in (10) and (11) for TM polarization:

$$\eta \mapsto \mathcal{U} = \mathbf{F}\eta \quad (12)$$

Full details about the numerical implementation of these equations can be found in the reference [14].

To solve the inverse problem of determining the profile function from the scattered field data, a naive approach is to try finding the inverse operator  $\mathbf{F}^{-1}$ . In practice however, such a direct approach proves impossible because of forward operator  $\mathbf{F}$  non-linearity.

### 3. INVERSE PROBLEM

#### 3.1. Fréchet Derivative of the Scattering Operator

To solve this inverse problem, Newton-Kantorovich linearization is considered. This is done by finding  $\mathbf{D}$  the Fréchet derivative of  $\mathbf{F}$  at  $\eta$  involved in the linear relationship:

$$\begin{cases} \mathbf{F}(\eta + \delta\eta) = \mathbf{F}\eta + \mathbf{D}\delta\eta + o(\|\delta\eta\|_2), \text{ as } \|\delta\eta\|_2 \rightarrow \mathbf{0} \\ \mathbf{F}(\eta + \delta\eta) - \mathbf{F}\eta = \delta\mathcal{U} \simeq \mathbf{D}\delta\eta, \end{cases} \quad (13)$$

Here,  $\delta\eta$  symbolizes a small variation of the profile-function and  $\delta\mathcal{U}$  the linked small variation of the scattered field. The expression of the linear operator  $\mathbf{D}$  can be deduced from the reciprocity theorem. In [23], it was introduced in far-field configuration with an illumination by plane waves. In this work, we adapt this approach to emission of the incident field and reception of the total field by electric dipoles, localized in the transition zone, and for a perfectly conducting rough surface. With an invariance axis, the Fréchet operator  $\mathbf{D}$  takes the following forms

$$\delta\mathcal{U}_{\mathbf{te}} = \mathbf{D}_{\mathbf{te}}\delta\eta \quad \delta\psi_{\mathbf{te}}^{m\ell} = \frac{-i}{\omega\mu_o} \int_{\Gamma} \partial_n \psi^\ell(\mathbf{r}) \partial_n \psi^m(\mathbf{r}) \delta\eta(\mathbf{r}) d\Gamma \quad (14)$$

in TE polarization, while in the TM case,

$$\delta\mathcal{U}_{\mathbf{tm}} = \mathbf{D}_{\mathbf{tm}}\delta\eta \quad \delta\partial_z \psi_{\mathbf{s}}^{m\ell} = \int_{\Gamma} \{\partial_t \psi^\ell(\mathbf{r}) \partial_t \psi^m(\mathbf{r}) - k^2 \psi^\ell(\mathbf{r}) \psi^m(\mathbf{r})\} \delta\eta(\mathbf{r}) d\Gamma \quad (15)$$

#### 3.2. Iterative Process

It is now possible to estimate the actual profile-function  $\eta_a$  of a rough surface for which we measure the data  $\mathcal{U}^{\text{mes}}$ , by building an iterative process of updating the profile at each step  $n$ :

$$\eta_n = \eta_{n-1} + \delta\eta_n \quad (16)$$

The correction  $\delta\eta_n$  is obtained by minimizing the cost functional  $\xi$ . It expresses in the sense of  $\mathcal{L}_2$  norm the error  $(\delta\mathcal{U} - \mathbf{D}\delta\eta)$  of the linear system of equations (Equation (13)). Therefore, we have:

$$\begin{cases} \xi(\delta\eta) = \|(\mathcal{U}^{\text{mes}} - \mathcal{U}^{n-1}) - \mathbf{D}_{n-1} \delta\eta\|_2^2 \\ \min \xi(\delta\eta) \Leftrightarrow \delta\eta = \delta\eta_n \\ \text{With: } \delta\eta_n = [\mathbf{D}_{n-1}^\dagger \mathbf{D}_{n-1}]^{-1} \mathbf{D}_{n-1}^\dagger (\mathcal{U}^{\text{mes}} - \mathcal{U}^{n-1}) \end{cases} \quad (17)$$

The † symbol stands for the transposed complex conjugation.  $\mathcal{U}^{n-1}$  in Equation (18) denotes the data associated to the best available estimation of the profile-function  $\eta_{n-1}$  computed thanks to Equations (8) and (9) in TE polarization and to Equations (10) and (11) in TM polarization. Unfortunately, the solution  $\delta\eta_n$  obtained at this stage is unstable. The inverse problem remains ill-posed because the continuity of the solution against data is not satisfied. Numerically, the consequence is an ill-conditioned matrix  $\mathbf{D}_{n-1}^\dagger \mathbf{D}_{n-1}$ . Noise due to model errors is thus amplified in the data ( $\mathcal{U}^{\text{mes}} - \mathcal{U}^{n-1}$ ). This leads to grossly erroneous estimation of  $\delta\eta_n$ . To overcome this difficulty, we introduce a mixture of zero and second order standard Tikhonov regularization [4]. The cost functional is thus changed from  $\xi$  to  $\tilde{\xi}$ :

$$\begin{cases} \tilde{\xi}(\delta\eta) = \|(\mathcal{U}^{\text{mes}} - \mathcal{U}^{n-1}) - \mathbf{D}_{n-1} \delta\eta\|_2^2 + \mu^2(\alpha \|\mathbf{S}\delta\eta\|_2^2 + (1 - \alpha) \|\mathbf{I}\delta\eta\|_2^2) \\ \min \tilde{\xi}(\delta\eta) \Leftrightarrow \delta\eta = \delta\tilde{\eta}_n \\ \delta\tilde{\eta}_n = [\mathbf{D}_{n-1}^\dagger \mathbf{D}_{n-1} + \mu^2(\alpha \mathbf{S}^\dagger \mathbf{S} + (1 - \alpha) \mathbf{I})]^{-1} \mathbf{D}_{n-1}^\dagger (\mathcal{U}^{\text{mes}} - \mathcal{U}^{n-1}), \end{cases} \quad (18)$$

$\mathbf{I}$  being the identity operator.  $\mathbf{S}$  stands for the second-order derivative operator such as  $\mathbf{S}[\delta\eta] = \frac{d^2}{dx^2}[\delta\eta(x)]$ . Both regularization terms serve to stabilize the solution by adding a constraint on the profile height and curvature, each weighted by the mixing parameter  $\alpha$ . Note that the regularization parameter  $\mu^2$  does not vary during the iterative process and its value is chosen by trial and error.

### 3.3. The First-Order Small Perturbation Method

The small perturbation method is the oldest and perhaps most popular method in wave scattering from rough surfaces. It is a perturbative expansion of the field scattered from a rough surface with respect to a small height over wavelength ratio. Derivation of that method for a one-dimensional perfectly conducting surface can be found up to the second order in many classical textbooks such as [24]. In such a classical derivation, incident field is a plane wave, while scattered field is approximated in the far-field regime. It is remarkable that Equations (14) and (15), when applied to a flat profile  $\eta = 0$ , form expressions of the first-order small perturbation method (SPM1) generalized to arbitrary incident and scattered fields.

Since the iterative process described in paragraph 3.2 is precisely started at first step  $n = 1$  from the horizontal plane  $\eta_0 = 0$ , the profile variation  $\delta\eta_1$ , solution of the linear problem (18), can be considered as a regularized inverse  $\eta_{SPM1}$  of the SPM1 approximate scattering theory. This profile  $\eta_{SPM1} = \delta\eta_1$  will be used in the Section 4 on numerical results as a representative of the approximate methods.

## 4. NUMERICAL RESULTS ON SYNTHETIC DATA

Synthetic data are generated with the forward model presented in Section 2. The number of points to describe the actual profile is  $\mathcal{N}_r = 5280$ . To avoid as much as possible an inverse crime, the profile estimated at each iteration is discretized with a different number of points  $\mathcal{N} = 2640$ . Note that this amount of data is much smaller than the number of points on the profile.

The emitters wavelength in the air is denoted  $\lambda$ , and is used as the length unit in the whole section. The number of emitters/receivers used is  $\mathcal{M} = 21$ . It consists in a set of electric dipoles located along a horizontal line piece with an interdistance  $d = 2.4\lambda$ , at a height  $h = 4\lambda$  from the average plane of the surface. Backscattering is disregarded, since the dipole cannot act simultaneously as an emitter and as a receiver. Therefore, the total number of redundancy-free scattered field data is equal to  $(\mathcal{M} - 1)\mathcal{M}/2 = 210$ .

The studied surfaces are realizations of a Gaussian random process with Gaussian spectrum [14]. The roughness is thus characterized by two statistical parameters, the height root mean square  $hrms$  and the correlation length  $lcor$ . For such a spectrum, the profile slope root mean square is simply given by  $srms = \sqrt{2}hrms/lcor$ . First, we set their root mean square height  $hrms = 0.095\lambda$  and we vary the correlation length in the range  $lcor \in [0.15; 0.5]\lambda$ . Second, the correlation length is fixed to  $lcor = 0.2\lambda$  and the root mean square height  $hrms$  is varied from  $0.08\lambda$  to  $0.14\lambda$ . Thus, the profiles root mean square slope  $srms$  lies between 0.26 and 0.99. The study is restricted to surfaces with the most pronounced roughness. The profile length is set to  $\mathcal{T} = 88\lambda$ . Note that the profile is flattened along its edges over a distance of twenty wavelength, thus giving a real size of its roughness equal

$\mathcal{T} = 48 \lambda$ . This flattening aims at suppressing numerical artefacts due to edge effects (see Sections 2 and [19]).

To monitor the iterative process, we introduced two convergence criteria, namely  $\text{REF}_n$  the residual error field and  $\text{REP}_n$  the residual error profile. They are both calculated in the sense of  $\mathcal{L}_2$  norm. The first is defined as the difference between the simulated data and the measured field, while the second gives the difference between the estimated profile and the actual profile:

$$\text{REF}_n = \|\mathcal{U}^{\text{mes}} - \mathcal{U}^n\|_2^2 / \|\mathcal{U}^{\text{mes}}\|_2^2 \quad \text{REP}_n = \|\eta_a - \eta_n\|_2^2 / \|\eta_a\|_2^2 \quad (19)$$

The main objective here is to test the ability of the algorithm to reconstruct the surface roughness by processing the data. We proceed in three different ways. First and second, a single-polarization data set is processed, that is TE or TM, respectively. Third, the profile is estimated from dual-polarized data, that is by processing simultaneously the TE and TM data sets.

In the TE-only and TM-only cases, the solution is obtained by minimizing the cost functional (Equation (18)), starting from the  $z = 0$  horizontal plane as the profile initial guess. For the TE data, we note that the residual error between the actual profile and the reconstructed profile (Figure 2(a)) increases continuously with decreasing correlation length.

For the TM data, we observe (Figure 2(a)) a same continuous behaviour until the correlation length reaches the value  $l_{\text{cor}} = 0.4 \lambda$ . At this point, the residual error increases suddenly giving an incorrect estimation of the profile.

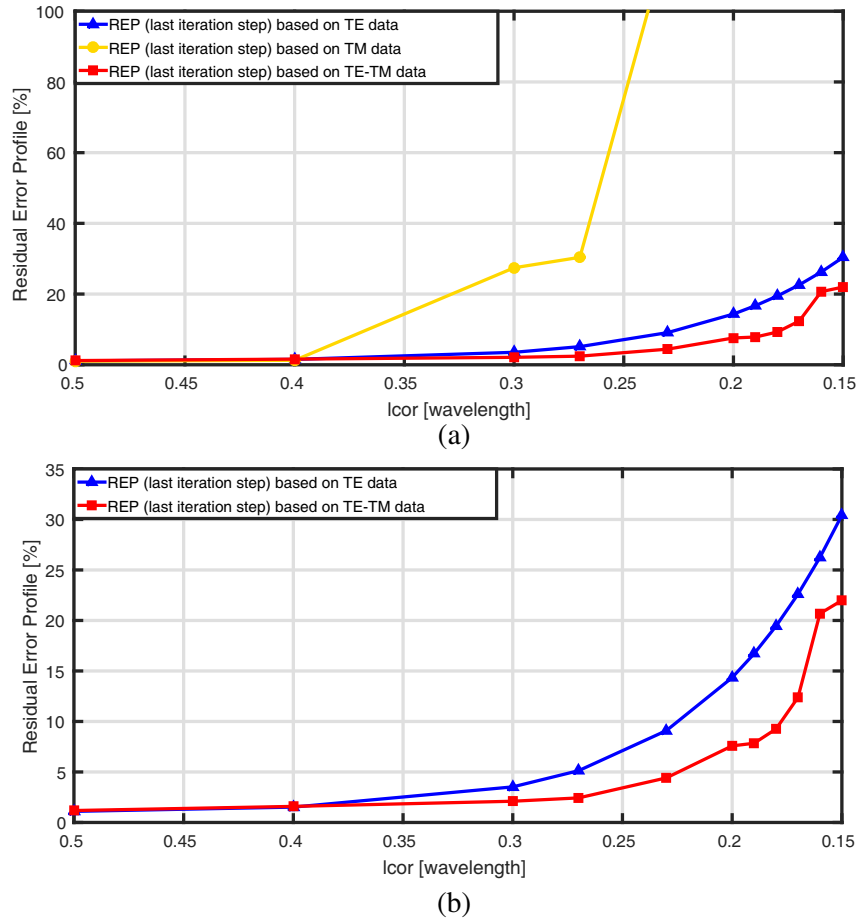


**Figure 2.** The last iteration step residual error profile as a function of the profile correlation length  $l_{\text{cor}} \in [0.15; 0.5]$  for a profile height root mean square of  $hrms = 0.095\lambda$ : (a) inversions of the TE data set, of the TM data set, and of the combined TE-TM data sets, and (b) zoom on inversions of the TE data set and of the combined TE-TM data sets.

In order to process TE and TM data together, we introduce a new weighting parameter  $\nu$  in the cost functional:

$$\left\{ \begin{array}{l} \tilde{\xi}^*(\delta\eta) = \|(\mathcal{U}_{\text{te}}^{\text{mes}} - \mathcal{U}_{\text{te}}^{n-1}) - \mathbf{D}_{\text{te},n-1} \delta\eta\|_2^2 + \nu^2 \|(\mathcal{U}_{\text{tm}}^{\text{mes}} - \mathcal{U}_{\text{tm}}^{n-1}) - \mathbf{D}_{\text{tm},n-1} \delta\eta\|_2^2 \\ \quad + \mu^2 (\alpha \|\mathbf{S} \delta\eta\|_2^2 + (1 - \alpha) \|\mathbf{I} \delta\eta\|_2^2) \\ \min \tilde{\xi}^*(\delta\eta) \Leftrightarrow \delta\eta = \delta\tilde{\eta}_n^* \\ \delta\tilde{\eta}_n^* = [\mathbf{D}_{\text{te},n-1}^\dagger \mathbf{D}_{\text{te},n-1} + \nu^2 \mathbf{D}_{\text{tm},n-1}^\dagger \mathbf{D}_{\text{tm},n-1} + \mu^2 (\alpha \mathbf{S}^\dagger \mathbf{S} + (1 - \alpha) \mathbf{I})]^{-1} \\ \quad (\mathbf{D}_{\text{te},n-1}^\dagger (\mathcal{U}_{\text{te}}^{\text{mes}} - \mathcal{U}_{\text{te}}^{n-1}) + \nu^2 \mathbf{D}_{\text{tm},n-1}^\dagger (\mathcal{U}_{\text{tm}}^{\text{mes}} - \mathcal{U}_{\text{tm}}^{n-1})) \end{array} \right. \quad (20)$$

With  $\nu^2 = 10^{-3}$ , the TM data weight is lowered in the algorithm, so that the reconstructed profile for short correlation lengths (Figure 2(b)) gets improved. Evolution of the residual error profile at short correlation length  $l_{\text{cor}} = 0.2 \lambda$  against the varying height root mean square is plotted in Figure 3. As usual, the  $z = 0$  plane is used as initial guess. For a profile which has a correlation length equal to  $l_{\text{cor}} = 0.2 \lambda$ , the behaviour of the two objective criteria ( $\text{REF}_n$ ,  $\text{REP}_n$ ) during the iterative process (Figures 4(b) and 4(c)), shows a significant improvement compared to the TE data inversion. Indeed, the depth of some hollows is poorly estimated with the first set of data (TE data), while a simultaneous use of all the data sets (TE-TM data), allows a reconstruction of almost all the hollows of the roughness and the finest details of the surface (Figures 4(a) and 4(b)). For both residual errors REF and REP, plots in Figures 4(b) and 4(c) clearly indicate that the first iteration solution (SPM1) is a very coarse estimation of the profile. Here, the SPM1 residual error profile reaches 70%. For this error to be reduced, the first dozen iterations appear particularly profitable.

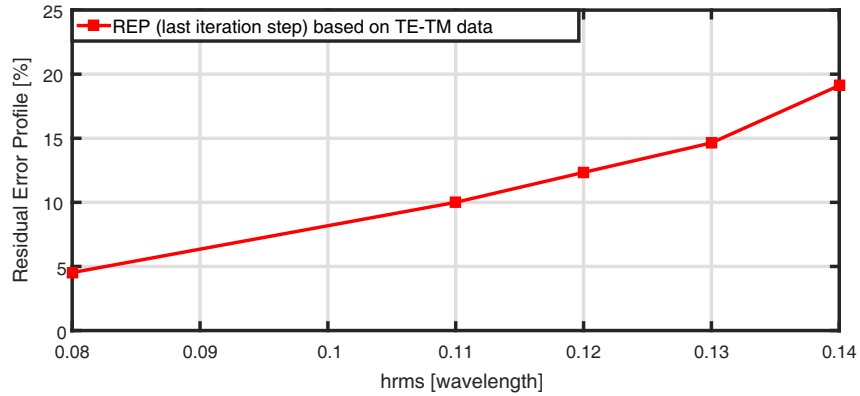


**Figure 3.** The last iteration step residual error profile as a function of the profile height root mean square  $hrms$ ,  $\in [0.08\lambda; 0.14\lambda]$  for a correlation length  $l_{\text{cor}} = 0.2\lambda$ : inversions of the combined TE-TM data sets.

To summarize those results on noiseless synthetic data, the residual error profile after one hundred iterations remains smaller than 2.5% for correlation length larger than  $0.3 \lambda$  (RMS slope smaller than 0.45), and smaller than 10% for correlation length larger than  $0.18 \lambda$  (RMS slope smaller than 0.75). These outstanding performances are obtained with our iterative process applied on dual-polarized data. Note that an inversion process of data under both polarizations takes around one hour run time for one hundred iterations. These simulations were performed using MATLAB with no particular optimizations on a personal computer, with a dual-core processor at 2.67 GHz and 4 Gb central memory.

For operational applications, it is essential to qualify the impact of noise on the performances of our inversion scheme. For this, some Gaussian noise is added to synthetic data generated for a profile with a correlation length  $l_{\text{cor}} = 0.3 \lambda$ . The signal-to-noise ratio is varied from 14 down to 6 (Figure 5).

Here, TE and TM data are processed simultaneously. In all cases, it is remarkable that the surface reconstruction process can be maintained convergent by adjusting the Tikhonov parameter to higher values. The algorithm can thus be adapted to the noise level, with the drawback that it becomes less sensitive to data. Still, the residual error profile that is 2.5% on noiseless data, rises up to 14% for a signal-to-noise ratio of 14, then 20% for  $\text{SNR} = 10$  and finally 31% for  $\text{SNR} = 6$ .

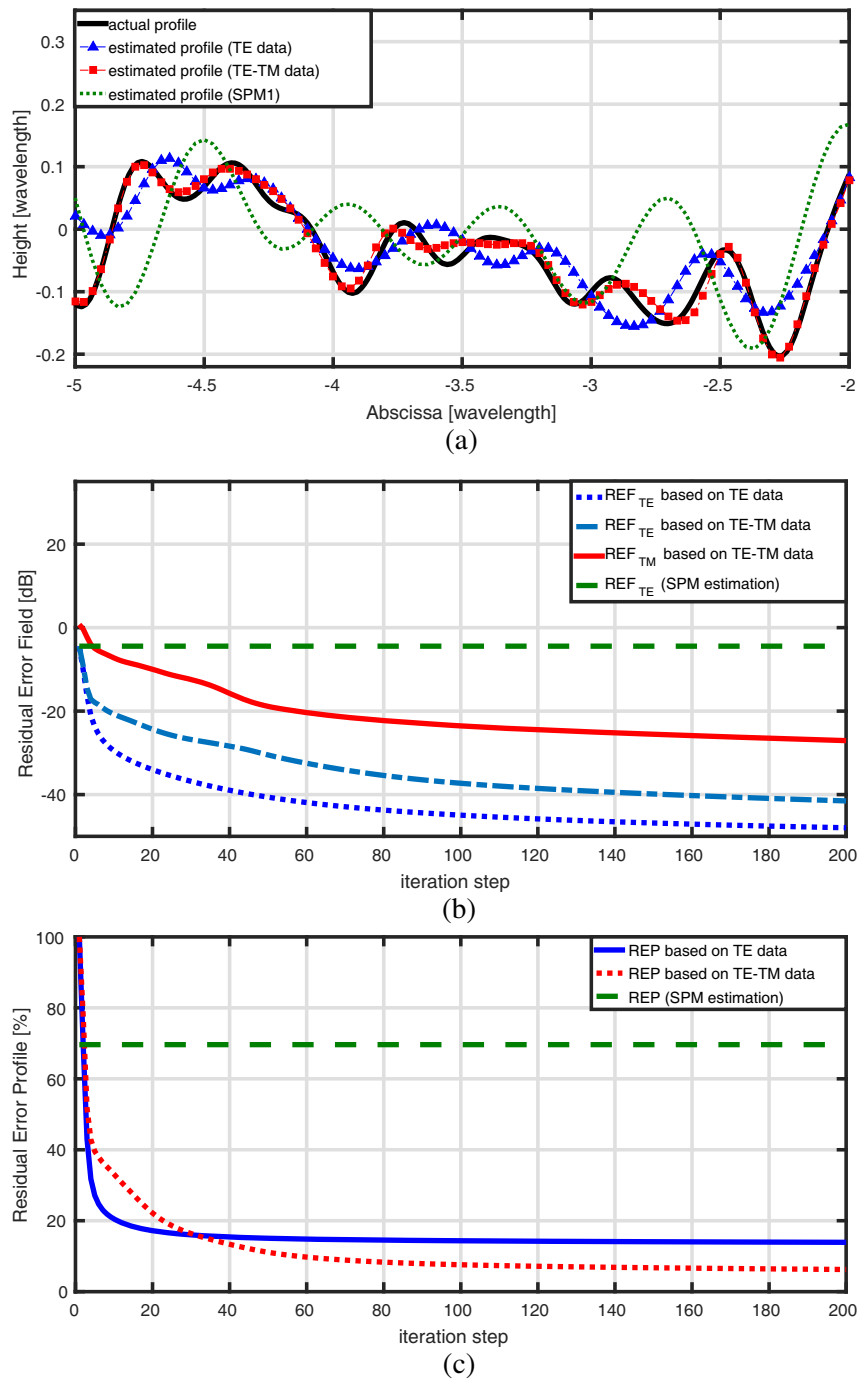


**Figure 4.** Inversion of noiseless synthetic data from a rough profile with statistical parameters  $hrms = 0.095\lambda$ ,  $lcor = 0.2\lambda$ : (a) comparison between the actual profile, the profile reconstructed from the TE data set, the profile reconstructed from the combined TE-TM data sets, and the SPM1 estimation of the profile from the TE data set, (b) the residual error field as a function of the iteration step for the TE data set, the TM data set and the combined TE-TM data sets inversions, and for the SPM1 estimation from the TE data set, and (c) the residual error profile as a function of the iteration step for the TE data set and the combined TE-TM data sets inversions, and for the SPM1 estimation from the TE data set.

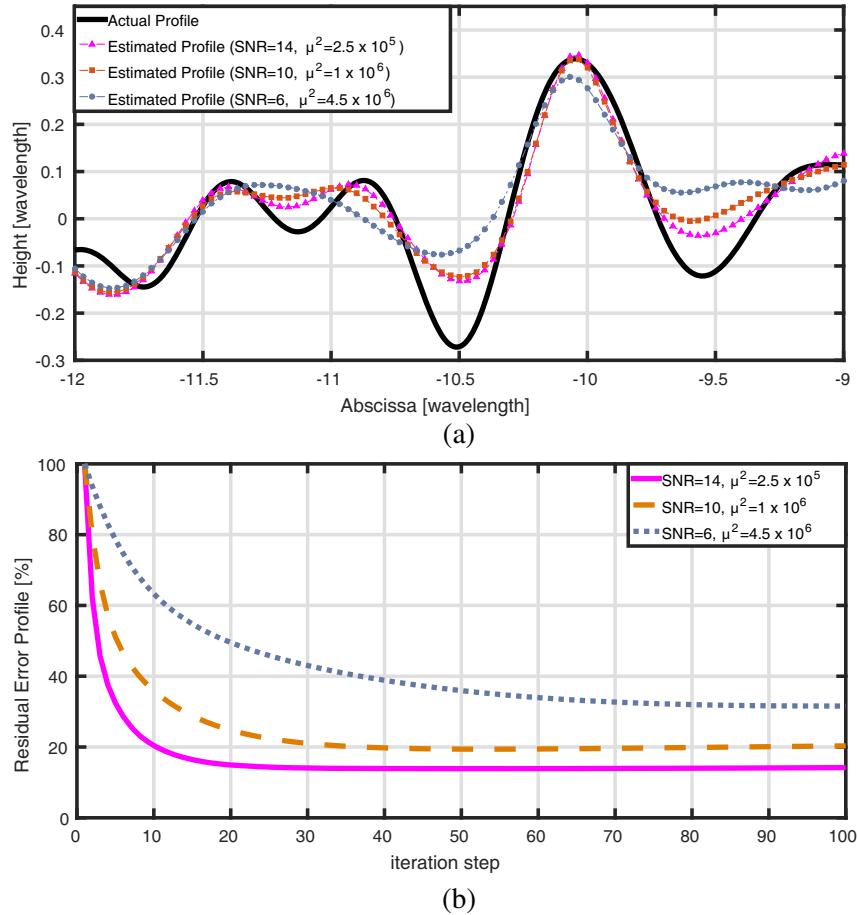


**Figure 5.** Inversion of noisy synthetic TE-TM data from a rough profile with statistical parameters  $hrms = 0.095\lambda$ ,  $lcor = 0.3\lambda$ : (a) comparison between the actual profile and the estimated profiles, and (b) residual error profile as a function of the iteration step. Three values of the signal-to-noise ratio are studied: 14, 10 and 6.

### 5. CONCLUSION

An effective inversion algorithm was proposed for reconstructing a one-dimensional perfectly conducting rough surface from electromagnetic wave scattering data. Those data correspond to the interactions between the rough surface and electric dipoles in the transition zone for both fundamental polarizations. The electric dipoles also play the role of receivers. For inversion, and contrary to several other approaches, the electromagnetic interactions are modeled rigorously following the boundary integral equation method. In such a numerical simulation, tapered waves are classically used to avoid spurious edge effects. However, localized sources in the vicinity of the surface do not radiate tapered waves. In this paper, the locally perturbed plane approach [19] was implemented to circumvent this obstacle.

Solving the inverse scattering problem consists in determining the best estimate of the actual profile from its scattered field. We implemented the Newton-Kantorovich iterative method. The calculus of the Fréchet derivative of the scattering operator is performed at each iteration step. Then, determining a new estimation of the profile involves the resolution of a regularized local linear inverse problem.

Gaussian rough profiles with height root mean square over electromagnetic wavelength ratio varying between to 0.05 and 0.14 and correlation length between 0.50 and 0.15 wavelengths are investigated, for a maximum slope root mean of 0.99. Numerical results show that such rough surfaces are poorly estimated by the first-order small perturbation method. This illustrates the need for inversion scheme based on a more advanced forward model, featuring multiple scattering. It also appear that TE and

TM data are not redundant, and should be systematically processed together to obtain the most reliable and stable solution. With the correct cost functional that mixes TE and TM data, we can show no counterexample where single-polarization inversion overperforms dual-polarization reconstruction. These results prove that the Newton-Kantorovich method can accurately inverse very rough surfaces, with correlation length much smaller than the electromagnetic wavelength. It should be pointed out that the residual error profile after one hundred iterations remains smaller than 2.5% for a profile with root mean square slope smaller than 0.45, and smaller than 10% for RMS slope smaller than 0.75.

Robustness to noise is checked and it appears that by adjusting the regularization parameter to the noise level, we can still get good quality reconstructions even at low values of the signal-to-noise ratio. For a profile with RMS slope of 0.45, the residual error profile is 2.5% on noiseless data, 14% for a signal-to-noise ratio of 14, 20% for  $\text{SNR} = 10$  and 31% for  $\text{SNR} = 6$ .

The inversion scheme presented in this paper can directly be applied to microwave measurements on metallic surfaces with an invariance direction. The first improvement that can enhance the practicality of the algorithm is to modelize the scattering diagram of the antennas. This is particularly easy and meaningful for the direct field between antennas. Extension to bad conductors or dielectrics, transparent or lossy, in the microwave regime is also at hand, since boundary integral equations and associated Fréchet operators exist for such boundary conditions. Finally, our approach is not limited to two-dimensional scattering. Numerical solutions for the forward problem on two-dimensional surfaces can be coupled to the locally perturbed plane approach [19]. However, with antennas on a grid and a two-dimensional surface, the size of matrix  $\mathbf{D}$  in the iterative process (Section 3) turns so large that specific numerical developments are to be planned.

## REFERENCES

1. Ulaby, F. T., R. K. Moore, and A. K. Fung, *Microwave Remote Sensing: Radar Remote Sensing and Surface Scattering and Emission Theory*, Vol. II, Reading, Artech House, MA, 1982.
2. Leach, R., *Optical Measurement of Surface Topography*, Springer, 2011.
3. Kress, R. and T. Tran, "Inverse scattering for a locally perturbed half-plane," *Inverse Problems*, Vol. 16, No. 5, 1541, 2000.
4. Tikhonov, A. and V. Arsenin, *Solutions of Ill-posed Problems*, Scripta Series in Mathematics, Winston, 1977.
5. Elfouhaily, T. and C. A. Guérin, "A critical survey of approximate scattering wave theories from random rough surfaces," *Waves in Random Media*, Vol. 14, R1–R40, 2004.
6. Mendez, O., A. Roger, and D. Maystre, "Numerical solution for an inverse scattering problem of non-periodic rough surfaces," *Applied Physics B: Lasers and Optics*, Vol. 32, No. 4, 199–206, 1983.
7. Wombell, R. and J. A. DeSanto, "The reconstruction of shallow rough-surface profiles from scattered field data," *Inverse Problems*, Vol. 7, No. 1, L7, 1991.
8. Afifi, S. and M. Diaf, "Scattering by random rough surfaces: Study of direct and inverse problem," *Optics Communications*, Vol. 265, No. 1, 11–17, 2006.
9. Wombell, R. and J. DeSanto, "Reconstruction of rough-surface profiles with the Kirchhoff approximation," *Journal of the Optical Society of America A*, Vol. 8, No. 12, 1892–1897, 1991.
10. Sheppard, C., "Imaging of random surfaces and inverse scattering in the Kirchhoff approximation," *Waves in Random Media*, Vol. 8, No. 1, 53–66, 1998.
11. Schatzberg, A. and A. J. Devaney, "Rough surface inverse scattering within the rytov approximation," *JOSA A*, Vol. 10, No. 5, 942–950, 1993.
12. Cmielewski, O., H. Torteil, A. Litman, and M. Saillard, "A two-step procedure for characterizing obstacles under a rough surface from bistatic measurements," *IEEE Transactions on Geoscience and Remote Sensing*, Vol. 45, No. 9, 2850–2858, 2007.
13. Ogilvy, J. A., *Theory of Wave Scattering from Random Rough Surfaces*, Adam Hilger, Bristol, 1991.
14. Tsang, L., J. A. Kong, K. H. Ding, and C. O. Ao, *Scattering of Electromagnetic Waves: Numerical Simulations*, Wiley Series in Remote Sensing, Wiley-Interscience, 2001.

15. Chew, W., M. Tong, and B. Hu, *Integral Equation Methods for Electromagnetic and Elastic Waves*, Morgan & Claypool, 2008.
16. Arhab, S., G. Soriano, K. Belkebir, A. Sentenac, and H. Giovannini, "Full wave optical profilometry," *JOSA A*, Vol. 28, No. 4, 576–580, 2011.
17. Arhab, S., H. Giovannini, K. Belkebir, and G. Soriano, "Full polarization optical profilometry," *JOSA A*, Vol. 29, No. 8, 1508–1515, 2012.
18. El-Shenawee, M. and E. L. Miller, "Multiple-incidence and multifrequency for profile reconstruction of random rough surfaces using the 3-D electromagnetic fast multipole model," *IEEE Transactions on Geoscience and Remote Sensing*, Vol. 42, No. 11, 2499–2510, 2004.
19. Spiga, P., G. Soriano, and M. Saillard, "Scattering of electromagnetic waves from rough surfaces: A boundary integral method for low-grazing angles," *IEEE Trans. Antennas Propag.*, Vol. 56, 2043–2050, 2008.
20. Meier, A. and S. Chandler-Wilde, "On the stability and convergence of the finite section method for integral equation formulations of rough surface scattering," *Mathematical Methods in the Applied Sciences*, Vol. 24, No. 4, 209–232, 2001.
21. Kantorovich, L., "On Newton's method for functional equations," *Dokl. Akad. Nauk SSSR*, Vol. 59, 1237–1240, 1948.
22. Roger, A., "Newton-Kantorovitch algorithm applied to an electromagnetic inverse problem," *IEEE Transactions on Antennas and Propagation*, Vol. 29, No. 2, 232–238, 1981.
23. Roger, A., "Reciprocity theorem applied to the computation of functional derivatives of the scattering matrix," *Electromagnetics*, Vol. 2, No. 1, 69–83, 1982.
24. Tsang, L., J. A. Kong, and K. H. Ding, *Scattering of electromagnetic Waves: Theories and Applications*, Wiley Series in Remote Sensing, Wiley-Interscience, 2000.